Challenges Toward a Cost-Effective Implementation of Optical OFDM

Mônica L. Rocha, Rafael J. L. Ferreira, Diego M. Dourado, Matheus M. Rodrigues, Stenio M. Ranzini, Sandro M. Rossi, Fabio D. Simões and Daniel M. Pataca

Abstract We present a review of concepts and challenges to implement the OFDM technique in the all-optical domain so that it may emerge, in a near future, as a technically and economically feasible option to meet, with spectral efficiency and energy saving, the ever-increasing demand of capacity in data transmission systems.

Keywords Optical communication · Optical OFDM · Optical fast fourier transform · Coherent detection

1 Introduction

Since the disruptive advent of erbium-doped fiber amplification and wavelength division multiplexing (WDM) in the early 1990s, it became common to justify most of the research on high capacity optical transmission systems as being motivated by the need to meet the ever-growing demand for bandwidth [1–3]. Nowadays, as services and applications continue to evolve, the growth in bandwidth demand still holds this argument valid, although in a more complex scenario that incorporates other equally important requirements such as increase of spectral efficiency (SE) and reduction (or better control) of energy consumption [4–9]. In this context, two multiplexing techniques stood out, among other advanced technologies that emerged, to meet the desired high spectral efficiency: optical orthogonal frequency division multiplexing

M. L. Rocha (✉) · R. J. L. Ferreira · D. M. Dourado
University of São Paulo, Av. Trabalhador São-carlense, 400, São Carlos, SP 13566-590, Brazil
e-mail: monica.rocha@usp.br

M. M. Rodrigues
Idea! Electronic Systems, Av. José Rocha Bonfim 214, Campinas, SP 13080-650, Brazil

S. M. Ranzini · S. M. Rossi · F. D. Simões
CPqD Foundation, R. Ricardo Benetton Martins 1000, Campinas, SP 13086-902, Brazil

D. M. Pataca
Universidade Paulista, Av. Comendador Enzo Ferrari 280, Campinas, SP 13045-770, Brazil
e-mail: daniel.pataca@docente.unip.br

A. Paradisi et al. (eds.), *Optical Communications*, Telecommunications and Information Technology, https://doi.org/10.1007/978-3-319-97187-2_8

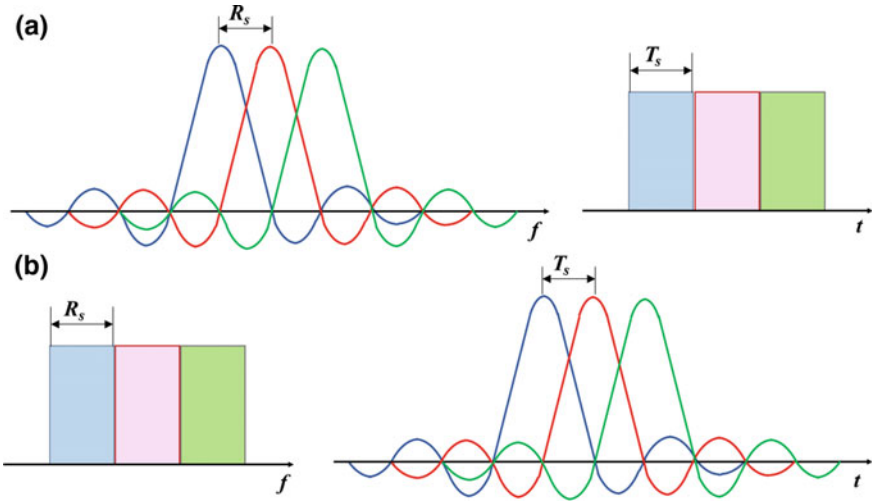

Fig. 1 **a** O-OFDM and **b** N-WDM signals represented in the frequency in time domains (R_S and T_S represent the symbol rate and duration, respectively)

(O-OFDM) and Nyquist WDM (N-WDM) [11, 12]. Both allow subcarrier overlapping—in the frequency and time domains, respectively, as illustrated in Fig. 1. Furthermore, both are typically associated with coherent detection and electronic processing that, by one hand, allow fulfilling the bandwidth specification but, on the other hand, increase the energy consumption [13, 14]. Note that, strictly speaking, there are two competing ways for implementing an OFDM signal in the optical domain: one refers to the electronic generation of an OFDM data stream (RF OFDM) that will modulate the optical carrier, usually called coherent OFDM (CO-OFDM) and more commonly investigated for access networking applications [10]. The other is associated to the modulation of optical subcarriers provided by an optical comb generator, thus comprising an all-optical OFDM data stream, hereby referred to as O-OFDM [12].

Despite the reciprocity in frequency and time of the two multiplexing techniques seen in Fig. 1, N-WDM with an adequate pulse shaping, in frequency, and overlapping, in time, has been proved to be a more reliable solution [14]. In fact, when compared to O-OFDM, N-WDM is a more mature technology that requires, among other advantages, a less complex transceiver and a lower ratio between transmitted peak power and average power [14–17]. Being able to minimize the occurrence of inter-symbol and inter-carrier interferences, ISI and ICI, respectively, N-WDM-based techniques usually employ wavelength selective switches (WSS) for optical filtering and channel selection with a reduced guard band between carriers. However, they still require a finite guard band between carriers, and whenever the need of a higher SE is more stringent, O-OFDM may represent a better option since it does not

require guard band—on the contrary, it allows spectral overlapping of subcarriers [12, 18, 19].

With that perspective in mind, in this chapter, we present an overview of concepts, challenges, and technological approaches for implementing the O-OFDM technique. The chapter focuses, mainly, on interferometric methods for the all-optical processing performed at the receiver side and at intermediate nodes [20–24]. This special attention is necessary because, as far as O-OFDM principles are concerned, demultiplexing, routing, adding, and dropping of optical subcarriers must be performed by mechanisms that do not violate the orthogonality condition. That is a feature intrinsic to the technique, and thus requires more sophisticated schemes allied to the conventional WSS. Mathematically, the interferometric methods operate similarly to the fast Fourier transform (FFT) and the inverse fast Fourier transform (IFFT) algorithms for providing a time-to-frequency conversion and a frequency-to-time conversion, respectively. To simplify the interferometric implementation in cases where the number of subcarriers increases, Hillerkuss et al. [21] proposed the use of optical filters combined with optical couplers, Mach–Zehnder interferometers (MZIs), phase shifters, and delay lines (DLs) and their proposal is explored in this chapter aiming at the design of more compact structures. Our main goal is to introduce a level of abstraction into a discussion that takes into account the fundamentals behind O-OFDM and N-WDM and disregards their present degrees of technological maturity. That could lead to a comparison between them based on the hypothetical assumption that both can be implemented by state-of-the-art technologies combining optoelectronics, optical/electronic processing of signal and integrated photonics. In that case, one could establish a pattern that, ultimately, relies on the energy consumption as a key factor for determining which technique should be employed in a case to case basis.

This chapter is organized as follows. Section 2 presents a review of OFDM fundamentals illustrated by the implementation of an electrical (RF) OFDM data stream that modulates an optical carrier and is recovered by a coherent receiver, comprising the so-called coherent OFDM (CO-OFDM). Section 3 describes briefly three common techniques used to generate an optical comb from a seed laser and the subsequent modulation of subcarriers, adequate to generate the mutually orthogonal subcarriers, i.e., the O-OFDM data stream. Section 4 focuses on the all-optical FFT and IFFT implementation. It starts by describing the complete interferometric technique before presenting Hillerkuss' simplification (Sect. 4.1), which leads to another approach based on the AWG technique [25] (Sect. 4.2). In Sect. 4.3, as a proof of concept, we describe an experiment configured with discrete components for demonstrating Hillerkuss' proposal applied for the drop of a subcarrier out of a four-channel O-OFDM [26]. In Sect. 4.4, the experimental results are used to calibrate a system simulator that performs the whole operation, thus including an all-optical IFFT for the insertion of a subcarrier [26]. Section 5 deals with synchronism and optical clock recovery of phase-modulated signals, illustrated by a technique based on the use of a four-wave mixing (FWM) process [27, 28]. In Sect. 6, we propose a node architecture, similar to those in [29–39] (Sect. 6.1) that summarizes what could be incorporated into a reconfigurable optical add and drop multiplexer (ROADM)

to enable the new functionalities. Finally, in Sect. 6.2, we present a brief discussion on energy consumption in Mach–Zehnder modulators implemented with integrated photonic technology [31–35], which will be necessary for allowing O-OFDM to become a cost-effective technique [36].

2 OFDM Fundamentals

The concept of (RF) OFDM was first introduced by R. W. Chang, in 1966, whilst the term "OFDM" first appeared in Chang's patent, in 1970 [37]. The most potential applications of the technique, however, would only be fully explored after the evolution of integrated circuits technology up to being able to support the computational effort required for a practical OFDM implementation. That became possible with the advent of broadband digital applications and very large-scale integrated (VLSI) CMOS chips, in 1990, which brought the technique into the spotlight [38, 39]. Since then, it has been extensively investigated mainly in the context of RF applications. Although its fundamentals remain the same whereas the optical domain is concerned, the translation from an RF OFDM signal, which will propagate through wired or, more typically, wireless channels, into its optical counterpart, which will propagate through an optical fiber, is not straightforward. That is because of intrinsic differences between the communication channels and the linear and nonlinear propagation effects that they induce. For example, in a linear propagation regime, multiple paths undergo a Rayleigh process in a typical wireless media, while in the optical media the phase dispersion caused by the fiber chromatic dispersion affects the propagation of multiple subcarriers in a different way [40, 41]. Although mentioned in this section, these linear effects are not addressed in details in a way to describe how exactly they are dealt with at the transmitter and receiver. Instead, the section will focus on more fundamental concepts and on a simplified mathematical formulation related to the generation and reception of a generic RF OFDM signal. In other words, it focuses on the digital signal processing techniques related to the Fourier transform. In the end, it will illustrate how a transmitter–receiver pairing can be implemented for allowing the propagation of a CO-OFDM signal.

OFDM is a special class of parallel transmission scheme, sometimes referred to as multicarrier modulation (MCM) [40, 41]. Conceptually illustrated in Fig. 2a, a generic MCM structure employs a complex multiplier (IQ modulator/demodulator) and requires an optimum detector, for each subcarrier, with a filter that matches the subcarrier waveform or, alternatively, a correlator matched to the subcarrier, as indicated in the figure. A classical MCM uses bandlimited signals that do not overlap and are generated by a large set of oscillators and filters at both ends. The major drawback of this approach is the excessive bandwidth it requires since the channel spacing has to be a multiple of the symbol rate, which reduces the spectral efficiency. OFDM, on the contrary, can be implemented by spectrally overlapping orthogonal signal sets, where the orthogonality originates from a correlation between any two subcarriers [40].

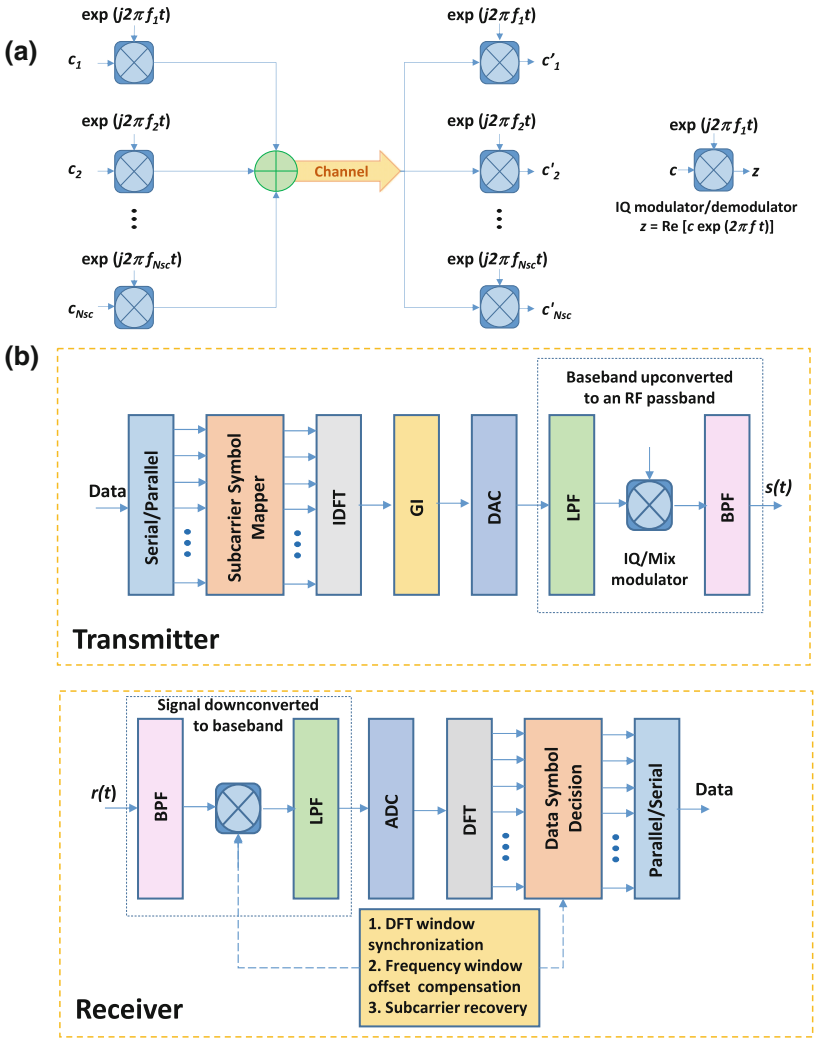

(i)DFT: (INVERSE) DISCRETE FOURIER TRANSFORM; **GI**: GUARD INTERVAL; **DAC/ADC**: DIGITAL-TO-ANALOG/ANALOG-TO-DIGITAL CONVERSION; BPF/**LPF**: BAND-PASS/LOW-PASS FILTER.

Fig. 2 **a** Schematic of a generic multicarrier system; **b** schematic of a generic OFDM transmitter and receiver for a point-to-point transmission (Adapted from [40])

According to the notation in Fig. 2a, for a transmitted signal, $s(t)$, c_{ki} is the i-th information symbol at the k-th subcarrier. This way, s_k is the waveform corresponding to the k-th subcarrier. Assuming that N_{sc} is the number of subcarriers, f_k is the subcarrier frequency, T_s is the symbol period, and $\Pi(t)$ is the pulse shaping function, it follows that [40]:

$$
\begin{aligned}
s(t) &= \sum_{i=-\infty}^{+\infty} \sum_{k=1}^{N_{sc}} c_{k_i} s_k (t - iT_s) \\
s_k(t) &= \Pi(t) \mathrm{e}^{j\,2\pi f_k t} \\
\Pi(t) &= \begin{cases} 1, \ (0 < t \leq T_s) \\ 0, \ (t \leq 0, t > T_s) \end{cases}
\end{aligned}
\tag{1}
$$

For a received signal, $r(t)$, in the time domain, the detected information symbol c'_{ki} at the output of the correlator is then given by [40]:

$$
c'_{ki} = \frac{1}{T_s} \int_0^{T_s} r(t - iT_s)\, s_k^* \mathrm{d}t = \frac{1}{T_s} \int_0^{T_s} r(t - iT_s)\, \mathrm{e}^{-j2\pi f\, t_k} \mathrm{d}t \tag{2}
$$

In a multicarrier system approach, a high-rate serial data stream is split up into a set of low-rate sub streams, each of which is modulated on a separate subcarrier (SC). In other words, a single data stream is transmitted over a number of lower rates SCs so that the bandwidth of the SCs becomes small compared with the bandwidth of the whole channel. The "key" concept of OFDM is, then, the spectral overlap allowed by selecting a special set of mutually orthogonal subcarrier frequencies, which thus provides the desired high spectral efficiency. The orthogonality originates from a correlation between any two SCs ("k" and "l") given by [40]:

$$
\begin{aligned}
\delta_{kl} &= \frac{1}{T_s} \int_0^{T_s} s_k s_l^* \mathrm{d}t = \frac{1}{T_s} \int_0^{T_s} \exp(j2\pi (f_k - f_l)) \mathrm{d}t \\
&= \exp(j\,2\pi (f_k - f_l)) \frac{\sin(\pi (f_k - f_l) T_s)}{\pi (f_k - f_l) T_s},
\end{aligned}
\tag{3}
$$

where, for an integer m, the orthogonality condition states that

$$
f_k - f_l = m \frac{1}{T_s} \tag{4}
$$

Figure 2b illustrates the implementation of other key concepts behind OFDM. The first states that the banks of I/Q modulators and demodulators, that would otherwise be required, can be replaced by signal processing algorithms. In that case, the inverse discrete Fourier transform (IDFT) and the discrete Fourier transform (DFT) algorithms can be used for, respectively, modulating and demodulating the data transported by the orthogonal SCs. To demonstrate this principle, we replace N_{sc} by N and assume that $s(t)$ is sampled at every interval T_s/N. The m-th sample of $s(t)$ may then be written as [40]

$$S_m = \sum_{k=1}^{N} c_k . e^{j2\pi f \frac{(m-1)T_s}{N}} \qquad \text{where} \quad f_k = \frac{k-1}{T_s} \tag{5}$$

Using the orthogonality condition (4), in (5), we then obtain [40]

$$s_m = \sum_{k=1}^{N} c_k \cdot e^{j2\pi f \frac{(m-1)T_s}{N}} = \sum_{k=1}^{N} c_k \cdot e^{j2\pi \frac{(k-1)(m-1)}{N}} = \Im^{-1}\{c_k\}, \tag{6}$$

where $\Im$ refers to the Fourier transform. Similarly, at the receiver, if the received signal $r(t)$ is sampled at every Tx/N interval, we will have [40]:

$$c'_k = \Im\{c_k\} \tag{7}$$

From (6) and (7), we notice that $s(t)$ corresponds to the N-point IDFT of c_k, and the received information symbol corresponds to the N-point DFT of the received signal. Note that, for a practical DFT/IDFT implementation, two devices are also essential: a digital-to-analog converter (DAC) that converts the discrete value of s_m to the continuous analog value of $s(t)$, and an analog-to-digital converter (ADC), that converts the continuous received signal $r(t)$ to the discrete sample r_m. This scheme can be implemented with relative simplicity using the fast Fourier transform (FFT) algorithm. Such simplicity comes from the algorithm's computational efficiency. In fact, since Cooley and Tukey's formulation in 1965, the FFT algorithm became a popular computational tool. That is because, as a DFT algorithm, it is able to reduce the complexity of computing a DFT from O (N^2) to O (N log N). In this representation, N corresponds to the data size and the big O is a classifying notation of the computational running time and/or space requirements [42].

Another key principle illustrated in Fig. 2b is the introduction, in the time domain, of a cyclic prefix known as Guard Interval (GI), to compensate the effect caused by a dispersive channel. As a consequence of its use, the transmitted signal becomes periodic and a time-dispersive effect (either in the wireless or optical channel) becomes equivalent to a cyclic convolution, discarding the GI at the receiver. A drawback of this technique is the loss of efficiency in transmitted power since the redundant GI must be also transmitted. At the receiver, the equalization (symbol de-mapping) required for detecting the data becomes an element-wise multiplication of the DFT output by the inverse of the estimated channel (channel estimation). For phase modulation schemes, multiplication by the complex conjugate of the channel estimate can do the equalization. Differential detection can also be applied where the symbol of adjacent SCs or subsequent OFDM symbols are compared to recover the data [41].

As a final remark related to the design of an OFDM receiver, time and frequency synchronization are also key issues because they are responsible for, respectively, identifying the start of the OFDM symbol and aligning the local oscillator frequencies at the modulators and demodulators. If any of these synchronization tasks are not performed efficiently and accurately, the orthogonality of the SCs may be lost, or at least partly lost, which will increase the penalties caused by ISI and ICI [41].

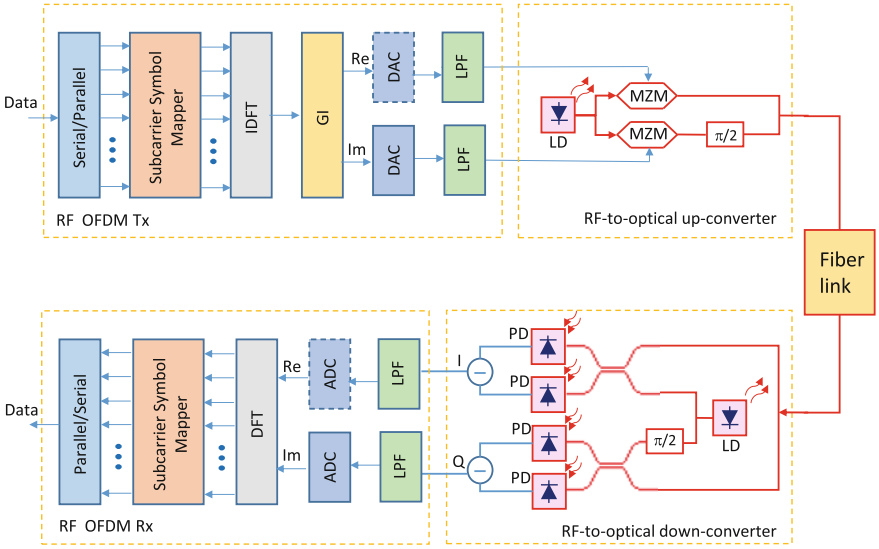

Fig. 3 Block diagram of a generic CO-OFDM transmission system with a direct up-/down-conversion architecture (Adapted from [40])

As a summary, Fig. 3 presents a conceptual diagram for implementing a generic CO-OFDM transmission system. It comprises five functional blocks: RF OFDM transmitter, RF-to-optical (RF-O) up-converter, optical link, optical-to-RF (O-RF) down-converter, and RF OFDM receiver [41]. For this basic setup, it is assumed a linear fiber propagation regime as well as a linear operation at the up- and down-conversion blocks. As illustrated, the input digital data at the Tx side are first converted from serial to parallel into a block of bits consisting of N_{sc} symbols, where each symbol consists of multiple bits for m-ary coding. These symbols are mapped into a two-dimensional complex signal c_{ki}. The RF OFDM signal in the time domain is obtained through the IDFT of c_{ki}. Next, a guard interval is inserted to avoid the channel dispersion. The digital signal is then converted to an analog form through a DAC and filtered by a low-pass filter that removes the alias signal. The subsequent RF-O up-converter transfers the baseband signal to the optical domain by using an optical IQ modulator comprising a pair of Mach–Zehnder modulators (MZMs) with a phase offset of 90°. The baseband RF OFDM signal is directly up-converted to the optical domain. After traversing the optical medium, the CO-OFDM signal is then fed into the O-RF down-converter, where it is converted to an RF OFDM signal again. Figure 2b shows the direct down-conversion architecture in which the intermediate frequency (IF) is near-DC. In the RF OFDM receiver, the IF signal is first sampled with an ADC. The signal then undergoes the three levels of synchronization: (i) DFT window synchronization: RF OFDM symbols are properly formatted to avoid ISI; (ii) frequency synchronization: frequency offset is estimated, compen-

sated, and, if possible, adjusted to a small value at the start; (iii) subcarrier recovery: each subcarrier is estimated and compensated [40].

3 O-OFDM Generation

The possibility of operating with only one optical source for generating multiple carriers represents a paramount issue for the O-OFDM technique and may favor it over N-WDM, where the operation of multiple laser sources is mandatory. In this context, a challenge for the O-OFDM design is to build up an optical multicarrier source where the orthogonality condition is always guaranteed. One way to assure the orthogonality relies upon the use of a single laser seed for generating phase-coherent frequency-locked subcarriers that will be synchronously modulated. As a bonus, the mechanism should also be able to guarantee the desired high aggregate capacity by exploiting parallel processing techniques, moderate modulation rate per subcarrier and high spectral efficiency.

A signal generated from such an arrangement is usually referred to as optical superchannel [12, 43]. Since the subcarriers are overlapped, the interference between them can be eliminated by avoiding frequency shifts of adjacent channels and that imposes another challenge, which is to adequately separate the subcarriers for individual processing. Therefore, a correct processing of one subcarrier out of several others requires that, at least, the following three conditions are met [43]:

1. The subcarrier separation must be equal to the symbol rate of each modulated subcarrier (that assures the orthogonality condition);
2. The symbols, in modulated subcarriers, must be aligned in time (thus fulfilling the synchronism requirement);
3. The transmitter bandwidth must be large enough to accommodate all subcarriers, provided that an appropriate sample rate and anti-aliasing filtering are applied (which satisfies the requirements for operation in an elastic optical networking context).

From the above conditions, it follows that for a given total symbol rate, the bigger the number of subcarriers the smaller the difference between their frequency separation and, consequently, the smaller the symbol rate that modulates each one of them.

Although a complete O-OFDM generation process undergoes two basic steps: generation of an optical comb and adequate modulation of subcarriers, this section is more concentrated on the optical comb generation stage. In previous works, we have experimental and theoretically investigated this subject in more details [43–46] but for the present scope it is enough to highlight that, from a number of optical comb generation techniques, proposed in the literature for this application, three have stood out as a promising base for more practical implementations:

1. **Cascade of Mach–Zehnder/Phase modulators (MZM/PM)**, seen in Fig. 4a: commonly used to generate signals with two to around eleven subcarriers—this

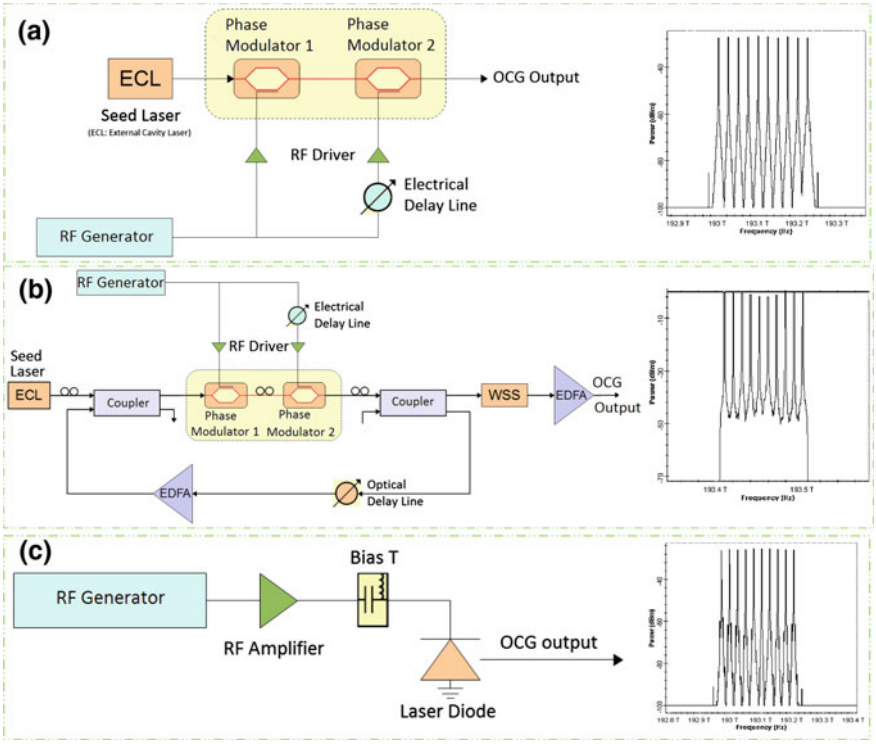

Fig. 4 Schematics of optical comb generators with their respective simulated spectrum: **a** cascade of Mach–Zehnder modulators; **b** recirculating frequency shifting (RFS); **c** laser gain switching (Adapted from [43])

limitation is determined by the MZMs/PMs electro-optic bandwidth and by the maximum amplitude of the driver signal. In this approach, two or more cascaded modulators are driven by phase-controlled sinusoidal electrical waves (tuned into the same RF frequencies). It is important to notice that not just MZ modulators may be cascaded, the setup may comprise a cascade of phase modulators (PM), or a combination of PMs and MZs. The important point here is that each modulator will produce a set of sidebands shifted by the RF frequency applied on the modulators. Another important aspect is that, in order to keep the overall optical to signal to noise ratio (OSNR) equalized, the amplitude of each subcarrier will have to be individually controlled [43, 47, 48].

2. **Recirculating Frequency Shifting, RFS**, Fig. 4b: based on the frequency conversion produced by single sideband modulation, allows the generation of a great number of stable subcarriers. In the RFS technique, a continuous wave (cw) laser signal is shifted, in frequency, within a recirculation loop due to an analog phase modulation process. In a basic configuration, the OCG consists of a seed laser, a 2×2 optical coupler, a double MZ modulator, an Erbium-doped fiber amplifier

(EDFA), to compensate for the loop losses, and an optical filter, for limiting the number of generated subcarriers and the level of amplified spontaneous emission noise (ASE) within the loop. The cw optical signal is continuously injected into the loop through one of the coupler input ports. After each round trip, part of the signal exits the loop and part returns to it. In the loop, the modulator is electrically driven by two mutually orthogonal RF sine waves. Its biasing points are adjusted in such a way to generate a single sideband suppressed carrier (SSB-SC) signal, which is then amplified and filtered. Note that the filter output is recombined with the signal seed laser signal, at the coupler input, so that, at each round trip, new comb lines may be continuously generated while the modulator output is continuously shifted by the RF frequency applied to the modulator. After many round trips, the initial comb lines are totally shifted to outside of the filter band; however, the process assures that new comb lines will be continuously generated inside the filter band. In the RFS spectrum, an excessive noise level is usually present, due to the use of optical amplifiers (EDFAs) required for the technique implementation [43, 49, 50].

3. **Discrete mode laser (DM) driven by a sine wave**, Fig. 4c: similar to gain switching in semiconductor lasers, results in phase locking at the comb output. Compared to the previous approaches, this one is relatively simpler and, consequently, of lower cost. In this implementation, a sinusoidal RF signal is amplified and directly applied into a laser designed for direct modulation applications. Its amplitude is adjusted for the desired optical to signal to noise ratio (OSNR) [43, 51–55].

The spectra seen in Fig. 4 were obtained from simulation pallets configured to equalize the comb lines by using a set of variable attenuators (VOAs) placed in between a DEMUX/MUX (WSS), as illustrated in Fig. 5. A generic O-OFDM generator thus comprises two basic stages: a seed-laser-based OCG and a modulation stage, consisting of a WSS (DEMUX/MUX) and modulation modules (MOD). If subcarriers' power equalization is necessary, VOAs may be included. The two experimental spectra illustrated in Fig. 5 were obtained with the RFS technique, taken at the DEMUX and MUX input and output, respectively [45].

4 Optical FFT/IFFT

Events in the time domain can be related to events in the frequency domain via the Fourier transform: going from time to frequency requires the Fourier transform itself, whereas the reverse process requires the inverse Fourier transform. This procedure can be implemented in several versions and the choice of which to use depends on the intended application. One of these applications is the signal processing performed with a sampled signal. At the limit, for a large spectrum tending to infinite, the sampling process causes different signals to become indistinguishable, an effect known as *aliasing*. On the other hand, at the time domain side, signals not limited

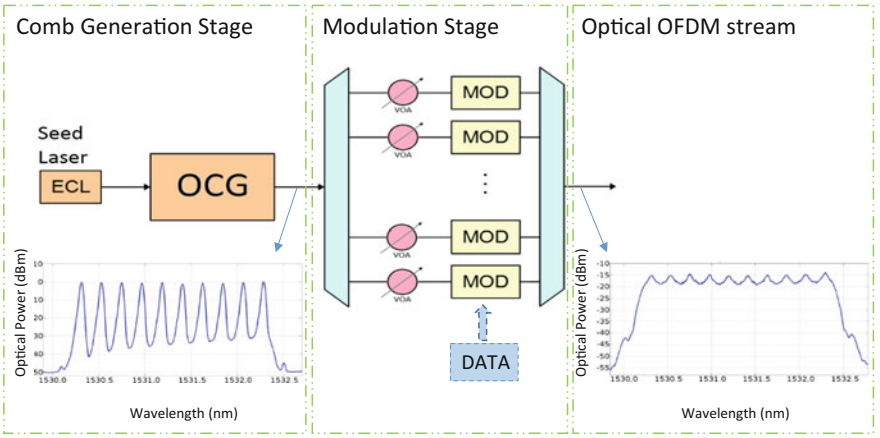

Fig. 5 Basic diagram of an O-OFDM superchannel generator comprising a seed-laser-based OCG and a modulation stage: WSS (DEMUX/MUX) plus modulation modules (MOD) (ECL: External Cavity Laser) (Adapted from [45])

in time lead to a processing that requires an infinite storage space [42]. Such a dual problem can be avoided by using the discrete Fourier transform (DFT), in which the signals are sampled in both time and frequency domains [42]. The fast Fourier transform (FFT) is merely a rapid mathematical method for computational applications of DFT. In this context, RF OFDM has become a prominence due to the ability of modern integrated circuits to generate this multicarrier signal by using IFFT and to reverse the process, in the receiver, by using FFT [42].

In a similar but not straightforward way, the O-OFDM approach depends on the maturity of a technology that will allow it to become as popular as RF OFDM. That, by inference, should be related to the optical counterpart of the (I)FFT algorithm implemented by an optical integrated circuit.

The use of integrated optics (IO) for implementing the FFT algorithm in the optical domain was first suggested by Marhic et al. in 1987 [56], although at the time the IO technology was not mature enough for practical demonstrations. Later, in 2001, Siegman et al. proposed a more achievable solution for obtaining the DFT of a sampled optical array that traversed a combination of optical 3-dB couplers and optical phase shifters [57]. Despite the difficulty to be implemented and stabilized in discrete assemblies, these interferometric types of structure have been studied for the processing of O-OFDM signals since then [58–65]. As they may suffer from complexity increase in their design as the number of subcarriers increase, in 2010 Hillerkuss et al. proposed a simplification in the interferometric method that could form a basis for the design of reliable and less complex schemes aiming at more cost-effective solutions [21]. In this same line of application, in 2011 Wang et al. proposed the use of conventional arrayed waveguide gratings (AWG) as integrated spectral filters to perform the optical FFT/IFFT functions [25]. Wang's proposal is

promising because, compared with other FFT/IFFT optical circuits, AWGs are less complex structures, especially for a large number of inputs and outputs [25].

4.1 Interferometric Technique

Consider a system with n inputs, m outputs and N time samples, where $N = 2^p$ and p is an integer. Furthermore, consider that x_n represents the time-series sample of a signal $x(t)$, taken over a period T, and X_m is the correspondent complex spectral components repeated with a period T. The N-point DFT transforming the N inputs x_n into N outputs X_m is then given by [21]:

$$X_m = \sum_{n=0}^{N-1} \exp\left[-j2\pi \frac{mn}{N}\right] x_n, \qquad m = 0, \ldots, N-1 \tag{8}$$

The FFT operates in such a way that it splits a DFT of size N into two interleaved DFTs of size $N/2$ after a number of recursive stages. That originates 'E_m' and 'O_m', the even and odd DFT of size $N/2$, for even and odd inputs x_{2l} and x_{2l+1} ($l = 0, 1, 2, \ldots N/2 - 1$), respectively. Mathematically, that can be expressed as [21]

$$X_m = \begin{cases} E_m + \exp\left[-j2\pi \frac{mn}{N}\right] O_m & \text{if } m < \frac{N}{2} \\ E_{m-N/2} - \exp\left[-j2\pi \left(m - \frac{N}{2}\right)\right] O_{m-N/2} & \text{if } m > \frac{N}{2} \end{cases} \tag{9}$$

In independent proposals, Marhic [56] and Siegman [57] demonstrated that, in order to obtain the spectral components of a time series, the N samples, taken at an interval T, must be fed simultaneously into an optical circuitry comprising a set of optical time delays acting as a serial-to-parallel (S/P) converter. This type of optical FFT (sometimes referred to as OFFT, or O-FFT) differs from the electronic implementation because it operates in a continuous mode and, to function correctly, the sampling must be performed in synchronization with the symbol over duration of T/N. This condition imposes a severe stability restriction and requires an extra care in maintaining equal delays and proper phase relations within waveguides that interconnect the optical couplers, thus configuring an interferometric structure. Despite these challenges, it is important to note that the optical FFT approach requires, mostly, passive devices with low power consumption in comparison with components of the electronic FFT approach. Furthermore, the fact that the optical sampling window sizes can be shorter than the electronic sampling windows (at the ADCs) gives to the optical FFT approach another important advantage.

This chapter focuses on Hillerkuss' proposal [21] because, besides the possibility of leading to simpler integrated devices, it may lead to a simpler experiment using discrete components. In fact, by working on both Marhic and Siegman's ideas, Hillerkuss et al. demonstrated that by reordering optical delays lines and relabeling

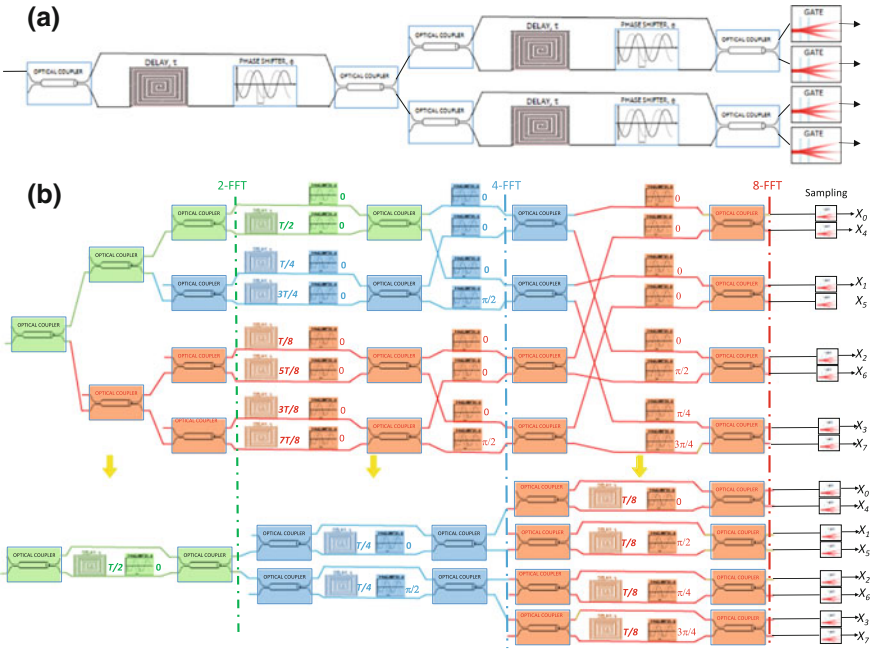

Fig. 6 **a** Four-point optical FFT in a low-complexity interferometric scheme; **b** complete interferometric method followed by the simplified version for $N = 2$, 4 and 8 (Adapted from [21])

outputs accordingly it is possible to simplify the overall structure of the optical FFT. Based on their development, Fig. 6a illustrates a setup for $N = 4$ [21]. Taking the initial approaches as a reference, this configuration was achieved after relocating the sampling gates to the end of the circuit, a step that does not change the overall operation. Furthermore, the delays in the S/P conversion stage were reordered and the outputs were relabeled accordingly in a way that the OFFT input could comprise two parallel delay interferometers (DIs). The simplification rules as proposed by Hillerkuss can be applied to any size (N) of FFT. Figure 6b illustrates the simplification process applied for $N = 8$, going from Marhic's scheme (top of Fig. 6b to the Hillerkuss' simplified version (bottom of Figure(b)) [21].

For applications that require add and drop functionalities, Hillerkuss' proposal offers an important advantage for the extraction of a single subcarrier. For that, once the subcarrier to be extracted has been selected, it is possible to remove all delay interferometers (DIs) that are not on the optical path that corresponds to the selected output port that leaves only one DI per stage, which leads to a number of DIs equal to $\log_2 N$. To select the subcarrier, it is only necessary to tune the phases in each DI, and that can be accomplished without changing the setup design, as illustrated in Fig. 7 [21].

Another important simplification proposed by Hillerkuss' aims at reducing one or more stages of DI by replacing them with standard optical filters [21]. The idea is

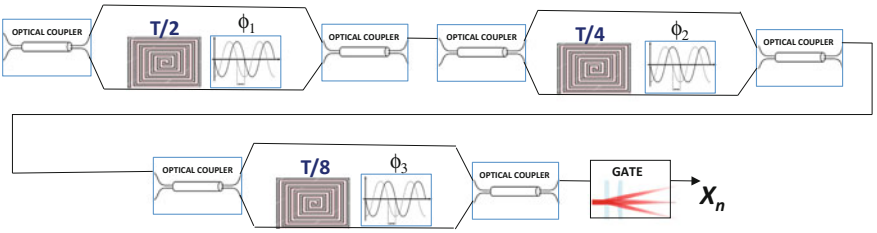

Fig. 7 Simplification principle: within a delay interferometer (DI), all delay lines (DL) that are not on the optical path correspondent to the selected output are removed (Adapted from [21])

based on the fact that the DFT acts as a periodic filter in the frequency domain with a free spectral range (FSR) equal to $N\Delta\omega$. Furthermore, each DI can be seen as a periodic filter with FSR $N\Delta\omega/2p$ where p is the index of the FFT stage and N is the order of the FFT. As a rule of thumb, the stages with a higher subscript (those being traversed last) have the largest FSR and should be replaced first. Figure 8 illustrates the technique for $N = 8$ [21].

4.2 AWG Technique

To further Hillerkuss' approach toward a popular device used as WDM MUX and DEMUX, Wang et al. proposed and demonstrated an all-optical FFT/IFFT scheme based on conventional arrayed waveguide gratings (AWGs) [25]. For this purpose, they showed, through simulated results, that it is possible to employ AWGs performing both functionalities, i.e., MUX/DEMUX and optical FFT/IFFT. That may be an important feature for an optical OFDM transmission that involves a large number of inputs and outputs. Wang's demonstration is based on a few additional conditions imposed onto the design parameters of a conventional AWG that operates as a WDM filter. Figure 9a illustrates a typical AWG with input/output waveguides, two focusing slab regions and one arrayed multichannel waveguide between two slab regions, with constant path increment ΔL between the channels. Usually, the two slab regions are identical with the details shown in Fig. 9b [25].

The basic design of such structure may be altered to include the optical FFT/IFFT functionalities in such a way to control the time difference of light traveling, τ, between adjacent channels in the arrayed waveguide, where $1/\tau$ defines the FSR in the frequency domain. The AWG can perform both optical FFT and IFFT operations by introducing a selection condition so that the AWG transmission spectrum repeats itself after every $N\Delta$ periods. In other words, the FSR of the AWG, $1/\tau$ matches exactly the spacing between different frequency bands, each band containing N channels. Such structures are named cyclic AWGs where the N arrayed waveguides provide temporal delays and the input/output slab regions produce phase shifts. The operation is only valid when all N copies of the signal, $s(t)$, overlap with

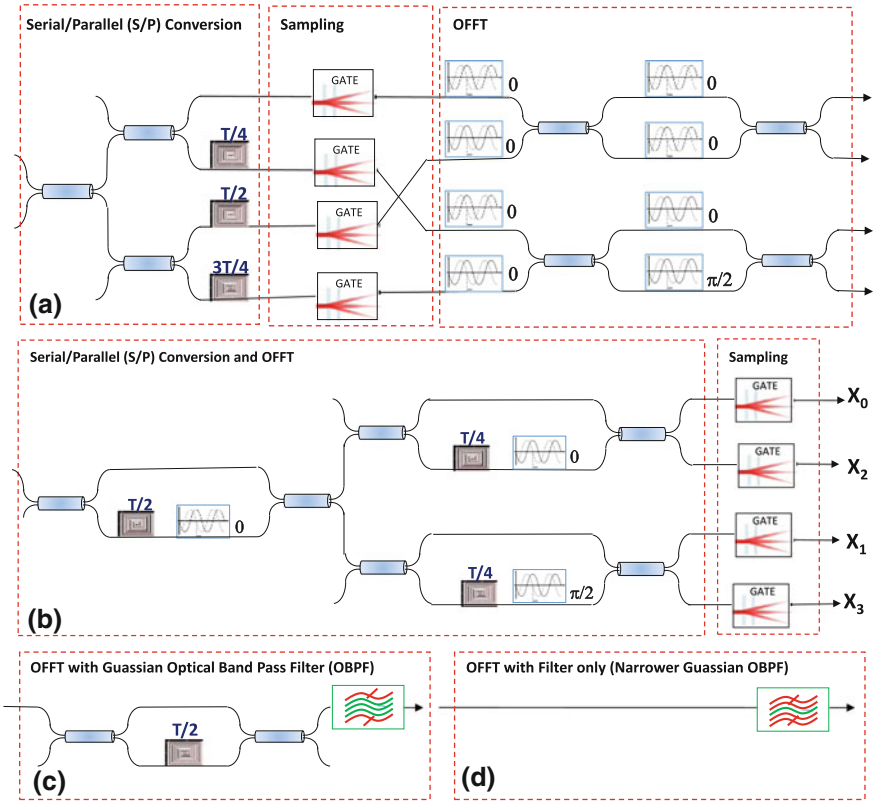

Fig. 8 **a** Optical FFT (OFFT) scheme for $N = 4$ points combining passive splitters and optical time delays for serial-to-parallel conversion. The optical gates sample the optical signal and the OFFT is obtained using 2×2 couplers and phase shifts; **b** after simplifications that eliminate redundancies and relocate the gates, a simpler scheme may be obtained; **c** technique for replacing parts of the DI by a first-order passband Gaussian filter wide enough to extract one subcarrier; **d** to replace more DI stages a narrower filter may be used but crosstalk and ISI may occur (Adapted from [21])

different time delay, i.e., there is only a time window with width τ, during which the FFT is realized. In this structure, a time gating device may be required to sample the signal at that window (as indicated in Fig. 10a). In the optical IFFT configuration (Fig. 10b), the input signal must be discrete at each subcarrier frequency, or at least have time interval less than τ. Otherwise, there will be ISI at some of the N samples caused by the time delay in the arrayed waveguide [25].

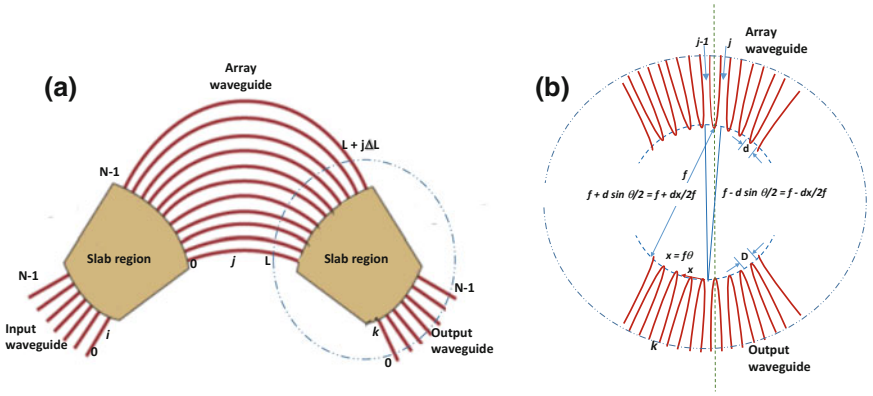

Fig. 9 **a** Typical AWG structure; **b** detail of its design where D is the AWG's input/output waveguide separation, the arrayed waveguide separation is d (for input) and d_1 (for output), and the radius of the curvatures is f (for input) and f_1 (for output). Here $d = d_1$, and $f = f_1$ (Adapted from [25])

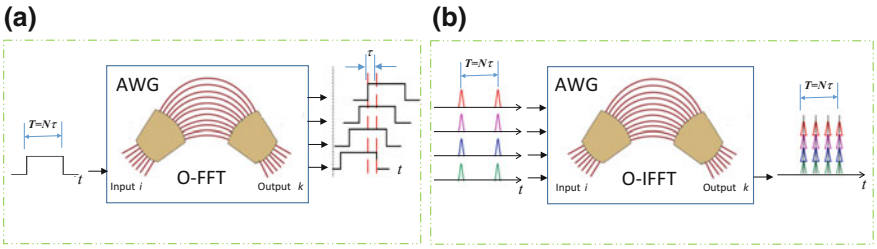

Fig. 10 Configuration of an AWG to operate as an optical. **a** FFT and **b** IFFT subsystem (adapted from [25])

4.3 Optical FFT Experimental Demonstration

In this section, we present the results obtained from a setup assembled for evaluating experimentally the *drop* stage of an optical FFT based on a discrete-component implementation, as illustrated in Fig. 11 [26]. The demonstration of an all-optical node that includes the *add* stage was simulated and will be presented in the next section. Despite having already investigated the OCG techniques based on a cascade of Mach–Zehnder and/or phase-modulators and also on the recirculating frequency shifter (rfs) techniques, for this proof of concept we used an OCG based on the gain switching of a semiconductor laser because of its simplicity and energy-saving potentiality. The generated comb lines can be seen in Fig. 11a, where the frequency spacing between the optical carriers, Δf, 12.5 GHz, imposes a bit rate equal to 12.5 GBd to satisfy the orthogonality condition. Due to its laboratorial availability, the modulation format used was quadrature shift phase keying (QPSK), which thus resulted in a bit rate of 25 Gb/s/subcarrier. Figure 11c illustrates the eye diagram

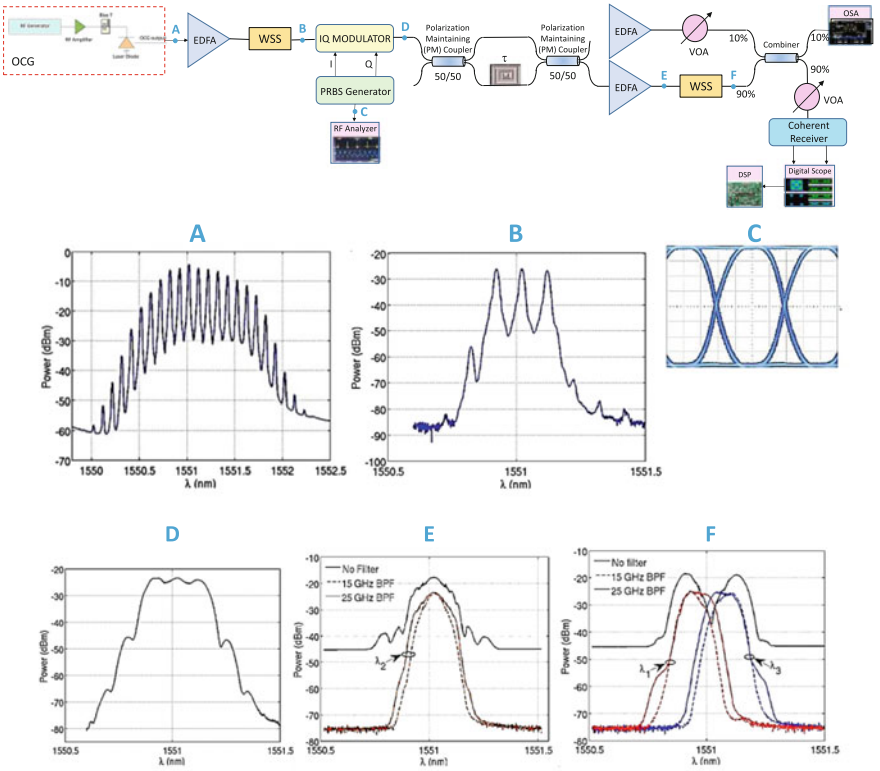

Fig. 11 OFFT experimental demonstration by dropping one subcarrier out of a three-subcarrier O-OFDM signal. The OFFT comprises a two-stage DI where the second one is replaced by a tunable bandpass filter wavelength shaper (WSS) (Adapted from [26])

of the modulating data at the PRBS generator output. Furthermore, as the need of using discrete components that are insensitive to polarization fluctuations limited the number of available couplers, the demonstration was performed with only three subcarriers (Fig. 11b), thus resulting in a gross rate of 75 Gb/s.

The optical OFFT demonstration was based on the scheme seen in Fig. 11, where the second DI stage was replaced by an optical bandpass filter. The assembling of the first DI required the use of an optical bench because the nonintegrated interferometric subsystem operated without a stabilization circuitry. For dropping one carrier out of the three-subcarrier signal, we used one delay line (DL), one splitter and one 2×2 coupler with polarization maintaining (PM) fibers, followed by a WSS replacing the second DI. Figure 11d–f show the spectra at the first DI input, second DI input (after the EDFA) and output, respectively. To evaluate the influence of crosstalk and ISI in the BER performance, caused by replacing the second DI by the filter, the WSS was set to two band values, 15 and 25 GHz so that we could select the best performance passband [26].

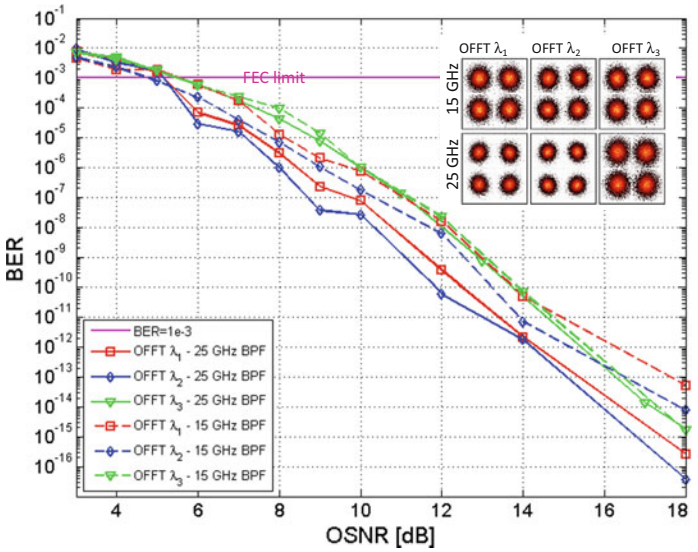

Fig. 12 (a) Experimental results (BER vs. OSNR) for each carrier dropped by the OFFT where one DI stage was replaced by a band pass filter (BPF) tuned to 15 and 25 GHz. Inset: constellation of the three dropped carriers (Adapted from [26])

To complete the setup, there was a coherent receiver together with an arrangement comprising an EDFA, a VOA followed by an optical coupler, a splitter and a polarization controller (not shown but necessary for accessing the received signal before its processing at the DSP [26]). The receiver was a commercial integrated coherent receiver (ICR) used for the reception of 28 GBd-QPSK signals. The two electrical ICR output signals were sampled at 50 GSa/s by a two-channel real-time scope (20 GHz band) for offline DSP. As an optical local oscillator, we used a tunable external cavity laser (ECL) with 100 kHz linewidth. The DSP subsystem included anti-aliasing filtering, ortho-normalization, resampling to two samples/symbol, time recovery, constant modulus algorithm (CMA)-based equalization (with 60 taps), and carrier/phase recovery. For taking into account the measurement fluctuations and for providing a better assessment of the system behavior, each measurement was repeated sixty times. From these data, we selected the five with best performance and averaged them. The results thus obtained are summarized in Fig. 12.

Figure 12 shows the BER versus OSNR for each carrier dropped by the OFFT using the BPFs configured to 15 and 25 GHz, as well as the constellation diagrams after the OFFT operation. The performance with the narrower band (15 GHz) was worse for the three carriers in comparison to their behavior with the wider band (25 GHz). That happened because the narrower band cut the high-frequency components of the signal, thus distorting its eye diagram. Note that for both pass bands, the central carrier (λ_2) presented a better performance than the side carriers (λ_1 and λ_3). One possible explanation for that behavior is the lack of symmetry, caused by

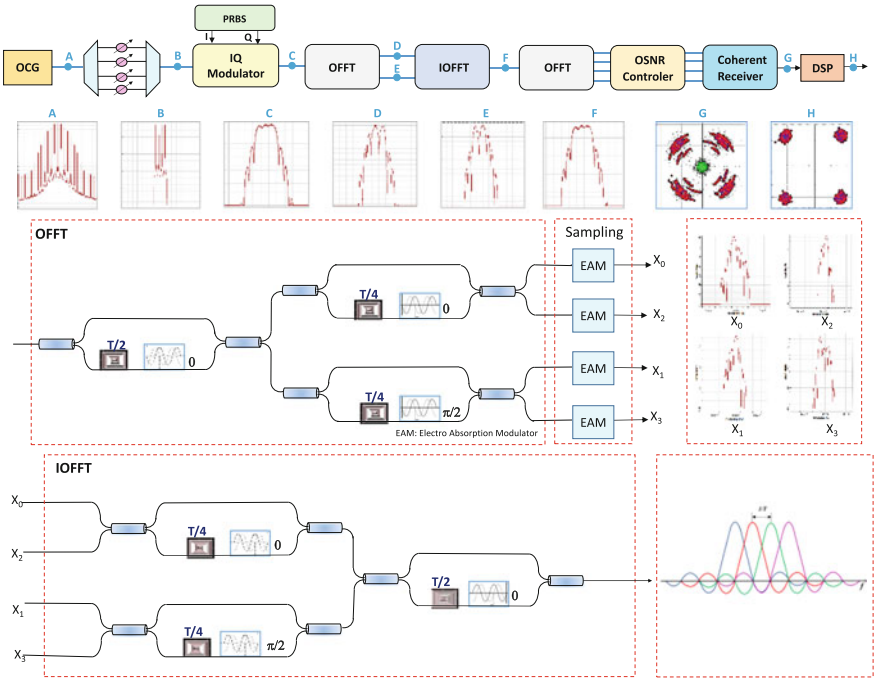

Fig. 13 Scheme for the all-optical FFT/IFFT/FFT processing of a four-subcarrier O-OFDM, as configured in a simulation pallet (Adapted from [26])

the absence of the fourth subcarrier, in the four-order OFFT implemented. Figure 12 also illustrates the constellation diagrams of the received carriers for the OSNR equal to 6 dB. Again, we can note the degradation of the dropped carriers when using the narrower filtering (15 GHz) [26].

4.4 Optical FFT/IFFT Simulated Demonstration

To validate the simulated results, a setup (Fig. 13) similar to the experiment was configured in a simulator (Optisystem 13.2). As the optical devices used in the experiment present a higher insertion loss, they required the use of optical amplifiers that could be avoided in the simulation but special care was taken to control the OSNR level. For the calibration, we used only one stage of DI and replaced the second stage by a Gaussian OBPF with (25 and 15 GHz).

As in the experiment, the best results were obtained for $\Delta f = 25$ GHz. Therefore, the results presented are all related to this bandwidth. We used a standard QPSK coherent receiver and DSP. At the receiver input, a block called "OSNR controller" was implemented to keep the OSNR at the same level of the experiment. However,

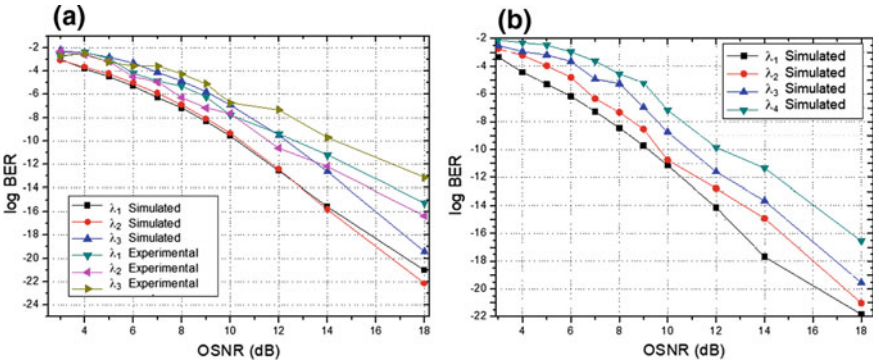

Fig. 14 **a** Simulated and experimental results (log BER vs. OSNR) for each subcarrier dropped by the OFFT and **b** a complete O-OFDM signal processing (dropping and adding) using the proposed all-optical FFT/IFFT interferometric technique in the simulation setup (Adapted from [26])

as expected, simulated results showed best performance and they did not take into account the unstable behavior of the experimental interferometers. All considered a comparison between experiment and simulation for the OFFT functionality shows a reasonable agreement for BER values up to ~10^{-12} (Fig. 14) [26].

Once validated, the pallet was adapted to include all DI stages, i.e., three stages wherein the first the delay is $T/2$. At one of its two outputs, a delay of $T/4$ was applied and combined with a phase shift of $\pi/2$, as indicated in Fig. 13. The $N = 4$ OFFT was then able to separate four subcarriers: X_0 and X_2 (the even subcarriers) and X_1 and X_3 (the odd ones). After the second DI stage, the four subcarriers were finally separated. For the next processing step (gate), we used electro-absorber modulators to sample each carrier. After that, the optical IFFT (similar to the optical FFT but with a reversed order of processing) was implemented. This whole procedure corresponds to the dropping and adding functionalities as it happens in an add/drop node. At the receiver, another optical IFFT was used for subcarrier selection, also tuned by the local oscillator laser. To complete the data assessment, a DSP analyzed the constellations and calculated the BER. The OSNR controller comprises an optical amplifier (to add noise) and an optical coupler.

The results for the four carriers, after being dropped, reinserted and received, are shown in Fig. 14 and their good BER versus OSNR behavior in a back-to-back configuration demonstrate the feasibility of the proposed technique applied to the O-OFDM signal processing [26].

5 Synchronization and Clock Recovery

Clock synchronization is another key step for implementing the O-OFDM technique and that can, in principle, be accomplished in two ways: asynchronously or syn-

chronously [66]. In the first, a received signal is used as a reference for detecting an offset between the clocks at the transmitter and receiver. The offset is then processed for further compensation, usually in a DSP. In a synchronous operation, the clock signal is extracted from the received signal, being, therefore, synchronized with it. Whenever coherent detection occurs, it is possible to use digital signal processing for performing the clock-related operation but, more generically, wherever synchronization is required, it may be more practical and costly if achieved in the optical domain [66–68]. For the O-OFDM approach, a challenge to be pointed out is that no matter the chosen clock recovery method, it should also satisfy the requirements of being simple, compact, easily integrated and low power consumer—that is not an easy task.

The all-optical process that takes place at a node or at the receiver of an O-OFDM superchannel system can be divided into steps. At first, the OFDM signal is demultiplexed by an optical IFFT module and, after that, a bank of optical gates (electroabsorption modulators, EAM) performs the time sampling of those subcarriers that will be dropped or rerouted. The optical gates are synchronized to a common clock, extracted from the superchannel. The availability of an analog clock is an important resource for enabling functionalities such as synchronization, phase tracking, and regeneration. One of the challenges in this particular part of the O-OFDM operation is to provide the desired clock signal disregarding the modulation format being used. In particular, for phase-modulated formats, recovering the clock from a signal is tricky. Aiming at that goal, there have been many proposals in the literature, among them, this section describes a method that exploits the all-optical signal processing based on the nonlinear effect of four-wave mixing (FWM) [27, 28].

To illustrate the technique, Fig. 15 shows a scheme where the O-OFDM subcarriers are spaced by Δf and modulated with a QPSK data [27]. Initially, Δf is filtered by a narrow filter that selects two adjacent channels. Note that only two subcarriers are necessary to recover the clock but, for simplicity, the entire superchannel could be used. As the FWM will result after beating the signal and a pump, the use of only two subcarriers minimizes the distance between the pump and signal. The filtered signals and a continuous wave (cw) pump are then combined and injected into the first stage of a SOA. As it takes place, the FWM gives rise to idlers, whose frequency and phase are governed by [27]

$$\begin{aligned} f_{\mathrm{I}} &= 2f_{\mathrm{S}} - f_{\mathrm{p}} \\ \phi_{\mathrm{I}} &= 2\phi_{\mathrm{S}} - \phi_{\mathrm{p}} \end{aligned} \tag{10}$$

where f_{I} and ϕ_{I} are the frequency and phase of the idler, f_s and ϕ_{s} are the frequency and phase of the signal, and f_{p} and ϕ_{p} are the frequency and phase of the pump. The two idlers have double frequency spacing, $2\Delta f$, and double phase modulation and are, by the process, converted into BPSK signals. These two generated BPSK signals are selected by another filtering and injected into a second SOA, together with a second pump. This second stage is equivalent to the first one, and hence the phase information on the generated idlers is doubled again, converting the signals into nonmodulated carriers spaced by $4\Delta f$. Finally, these two idlers are filtered and

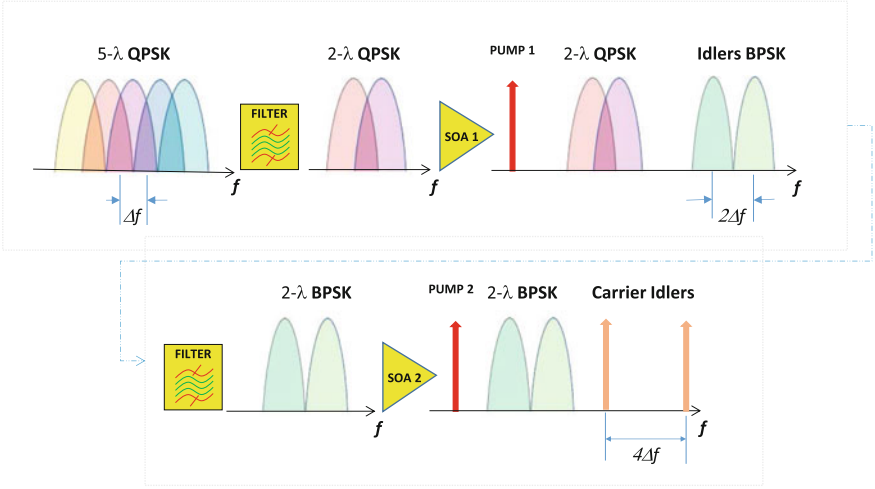

Fig. 15 All-optical clock recovery for an optical OFDM QPSK-modulated technique (Adapted from [27])

launched into a photodiode, where they beat with each other to produce a clock at a frequency of $4\Delta f$. In the electrical domain, this clock is down-converted, thus resulting in the original clock with frequency Δf [27].

6 Final Discussion

To conclude, this section presents a schematic view that integrates the parts described in the previous sections. In this way, it becomes possible to glimpse the transmission and reception structures as well as a node architecture, which can serve as a reference for an integrated photonic design aiming at overcoming the challenges for making O-OFDM an economical and technically feasible alternative.

6.1 O-OFDM Node Architecture

Figure 16 shows a proposal for combining the OCG-, clock recovery-, gating-, and optical FFT/IFFT- subsystems in a way to assemble an O-OFDM transmitter, an O-OFDM Intermediate node (ROADM) and an O-OFDM receiver. These diagrams give a better idea of how the subsystems can be integrated. Provided that it is guaranteed, the integrated structure design must be driven by requirements of operation stability, number of interconnections reduction and energy consumption optimization.

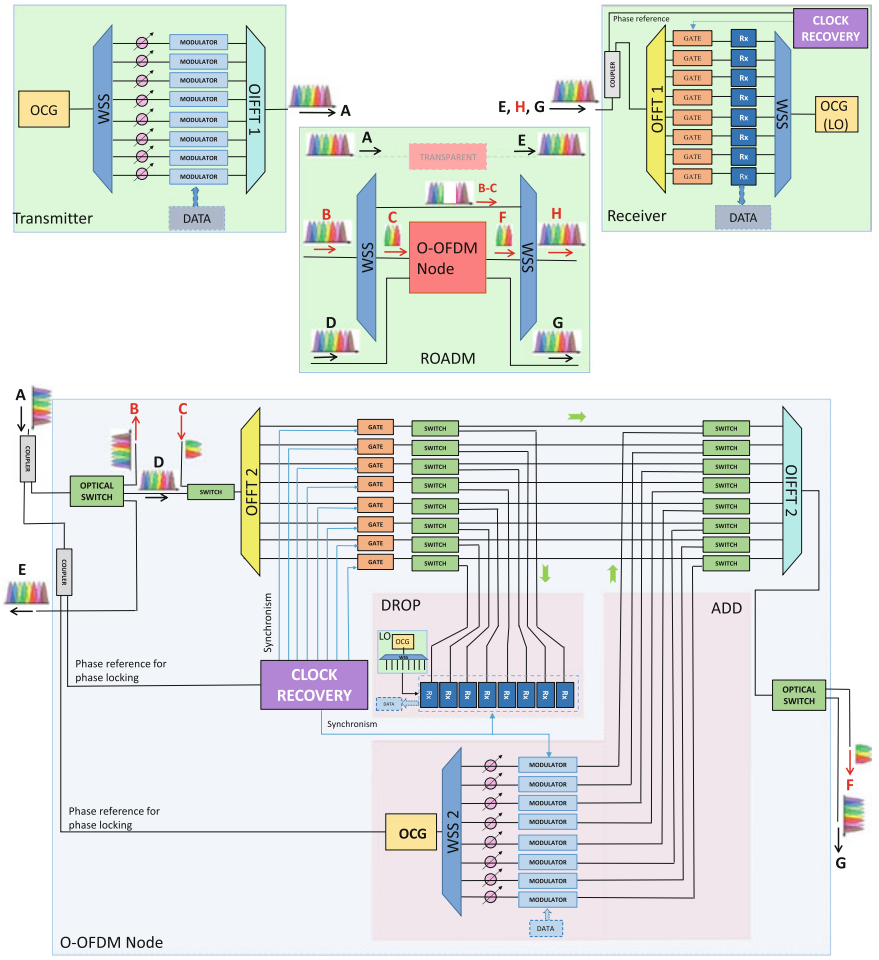

Fig. 16 Proposed architecture for assembling an O-OFDM transmitter, receiver and intermediated ROADM O-OFDM node

As illustrated in Fig. 16, the transmitter module comprises an OCG stage, one WSS, a modulation stage, and an OIFFT module (OIFFT 1). The WSS is used to separate the comb lines before their individual equalization and modulation. After that, the OIFFT module combines the mutually orthogonal subcarriers in order to generate the O-OFDM stream (A).

At the intermediate node input, an optical switch may connect the arriving super-channel to a WSS, for a sub-band selection, prior to the O-OFDM processing (B), or directly to the O-OFDM node, for local processing of as many subcarriers as required (D), or to bypass the intermediate node (O-OFDM node) by routing the whole data

stream to a next node or to a receiver (E) in a way that the ROADM O-OFDM node becomes transparent to the superchannel propagation.

The receiver stage comprises an OFFT module (OFFT-1) and individual coherent receiver setups (Rx), synchronized by the clock recovery module, where the local oscillator is provided by an OCG module.

If the O-OFDM stream is to be processed partially (C) or totally (D) at the intermediate node, the function of local extraction (dropping of subcarriers) and insertion (adding of subcarriers), controlled by a bank optical switches, may be performed as indicated by the green arrows. For that operation, after the subcarriers' separation, performed by the OFFT-2 module, a clock recovery module provides synchronism to gates, modulators of locally generated subcarriers and receivers. Usually, electro-absorption modulators perform the sampling operation (gates), necessary for extraction of subcarriers. The OIFFT module (OIFFT 2) combines the subcarriers, generated at the local OCG, which will be modulated and inserted into the traversing O-OFDM superchannel. Note that the local OCG must be phase locked with the O-OFDM entering the node and, for that, a phase reference may be used as indicated. Alternatively, and for routing purposes, the optical switches may include more WSS's for band selection (at the input) and band recombination (at the output) for dropping/adding or routing of subcarriers in a passband, while the remaining subcarriers just traverse the node.

As it can be inferred from the proposed architecture and the description of its modules presented in previous sections, there is still a long road in integrated photonics' design to be crossed before reaching the cost-effective target. However, the path is relatively clear and recent advances, especially in the design of waveguide structures such as modulators, delay lines, and phase shifters, when integrated with optoelectronic devices, point toward a promising near future for O-OFDM [63, 69].

6.2 A Few Remarks on Technical and Energy-Saving Feasibility

No matter, if applied to O-OFDM or N-WDM, it will be always convenient to replace high power consumption technologies (based, for instance, on high-speed digital signal processing) by all-optical signal processing techniques that represents a potentially energy-efficient alternative to their electronic counterpart either for N-WDM of O-OFDM. For this reason only, the research on all-optical signal processing is justifiable, especially when applied for also enhancing the spectral efficiency. That is the context for developing all-optical OFDM technology because it employs a great number of passive devices, such as optical delay lines, optical phase shifters, optical filters, and optical couplers, usually connected in interferometric configurations. The research on this area has been carried out by many groups that report different designs including such elements. Usually, the designs are based on silica planer light-

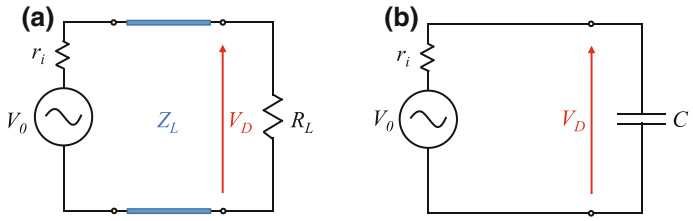

Fig. 17 Example of an equivalent circuit for an electro-optical modulator combined with **a** resistive load and **b** capacitive load (Adapted from [75])

wave circuit (PLC) and must fulfil requirements that go beyond the device operation [31–35, 69].

Particularly, for photonic modulators, which seem to be the core devices for the optical OFDM implementation, the electrical energy consumption to operate the modulator is a critical issue. As related in [70], the power required to operate the device increases with the modulation frequency, and can be measured by the ratio of the operating power per bandwidth unit. Usually, this figure of merit is expressed in watts per hertz [70] or in joule per bit [71]. Energy efficiency has been emphasized in recent years as one of the most important metrics of interfaces involving photonic circuits and electronic circuits. By verifying the state of the art in photonic devices, studies show that the best alternative for energy consumption is focused on electro-optic (EO) modulators, as can be seen in [72–74]. The energy consumption of an EO modulator depends on the physical properties of the phase shifters and the electronic design of the driving circuits. Figure 17 shows two examples of equivalent circuits used to measure the power consumption in electro-optical modulators.

Conventionally, some modulators are designed as traveling wave devices, which have 50 Ω input impedance (r_i) combined with 50 Ω impedance of the transmission line and RF cables (Z_L), in order to achieve maximum power transfer to the transmission line (see Fig. 17a). In this case, the driving voltage (V_D) is only half the voltage of the open circuit source (V_0). Therefore, for a simple OOK modulation format, for example, the energy consumption per bit ($E_{\mathrm{bit,\,R}}$) in the modulator can be estimated by considering the energy dissipation in the load resistor (R_L) during a bit duration slot (T_bit) [75].

$$E_{\mathrm{bit,R}} = \frac{V_\mathrm{D}^2 \times T_\mathrm{bit}}{4R_\mathrm{L}} \tag{11}$$

Thus, if we consider $V_\mathrm{D} = 1$ V, $R_\mathrm{L} = 50$ Ω, a bit rate of 10 Gb/s and a bit duration equal to 100 ps, for example, the energy consumption per bit will be 500 fJ/bit [75].

On the other hand, according to Koos et al. [75], this energy consumption can be reduced by using silicon–organic hybrid (SOH) modulators, since the phase shifters of these structures can be manufactured in much smaller dimensions than devices based on the free-carriers dispersion. As a consequence, the length of the SOH modulators phase shifters can be short compared to the RF wavelength of the modulation

signal, so that the device does not need to be designed in a traveling wave configuration combined with impedance. Assuming that the electronic driver circuits can be integrated in close proximity so that the circuit power lines can be kept short and the impedance is not required, these modulators (SOH) can be operated by purely capacitive loads, as shown by Fig. 17b.

Considering a SOH modulator operating below its cutoff frequency ($f_c = 1/2\pi r_i C$), the driving voltage reaches a permanent state value equivalent to $V_D = V_0$. Thus, the energy consumption will be related to the energy dissipation in the resistor r_i during the charging and the discharge of the capacitor (C). For a NRZ-OOK modulation format, for example, the power consumption per bit ($E_{bit,\,C}$) in this modulators class is given by [75]

$$E_{\text{bit},C} = \frac{V_D^2 \times C}{4} \tag{12}$$

Considering $V_D = 1$ V and a phase shifter of 500 μm, which has capacitance of 200 fF, for example, the energy consumption per bit ($E_{\text{bit},\,C}$) can be estimated at 50 fJ/bit. Note that, when compared to the value of the previous traveling wave example, this value is 10 times lower in magnitude [75].

To illustrate a design of integrated photonics applied to the optical OFDM operation, Fig. 18 shows an all-optical eight-channel OFDM demultiplexer (O-FFT) based on an integrated silicon-on-insulator (SOI) technique using PLC implemented by Hai Yu et al. [76]. Basically, the structure combines three-stage cascaded MZIs, and adjacent stages of the MZIs are connected by a directional coupler. The differential path length of each stage MZI is designed in a way that the first stage has the longest length, the second stage has a length half of that of the first stage and the third stage has a length half of that of the second stage. On one arm of each stage MZI, there is a phase shifter, which is used to tune the phase difference between the two arms. With the specific phase difference on each stage MZIs as shown, the eight channel outputs would be the demultiplexed OFDM signal in eight different subcarriers. More details on the design, fabrication and performance of the device may be found at [76].

In summary, we started the chapter with the premise that it should be possible to relate O-OFDM and N-WDM in a fairer comparison basis that assumes that both techniques can be implemented with similar technologies that would allow an evaluation of circuitry complexity and its associated energy consumption for both cases. Before this accurate comparison becomes possible, however, some challenges have yet to be overcome and we believe that the evolution of PLC design to integrate passive optical components and optoelectronic devices will soon allow surpassing most of these obstacles. Furthermore, regardless the integration challenging aspect, some subsystems still require a conceptual improvement in the sense of reducing complexity (that will also lead to reduced energy consumption). In this sense, an example of a technique that still requires improvement is the clock recovery. In some approaches, it may demand the use of one or two pumping lasers (and, in some cases, additional EDFAs) associated with SOAs to guarantee the power levels necessary for providing an efficient FWM process.

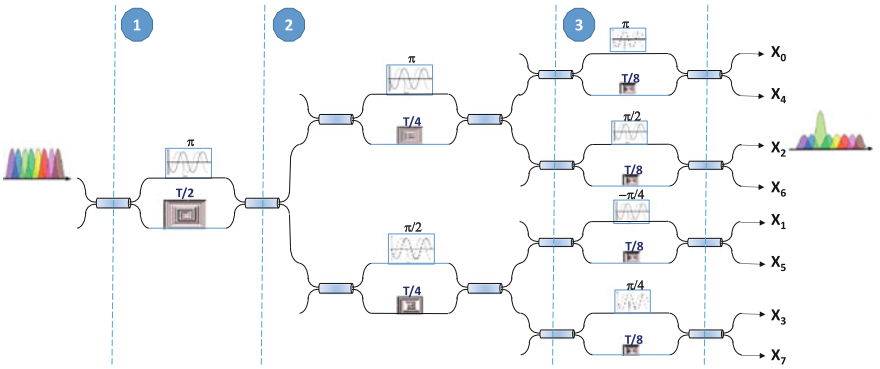

Fig. 18 Optical FFT structure (DEMUX) based on a three-stage MZI implemented on integrated SOI by Yu et al. (Adapted from [76])

In spite of challenges yet to be faced, the spectral efficiency, the potentiality for reducing the energy consumption and for tolerating linear fiber impairments, such as those induced by chromatic dispersion (CD) and polarization mode dispersion (PMD), continue to guarantee to O-OFDM a place of relevance in the group of technologies for very high capacity systems.

References

1. Keiser GE (1999) A review of WDM technology and applications. Opt Fiber Technol 5:3–39
2. Becker PC, Olsson NA, Simpson JR (1999) Erbium-doped fiber amplifiers fundamentals and technology. Academic Press, San Diego
3. Desurvire EB (2006) Capacity demand and technology challenges for lightwave systems in the next two decades. J Lightwave Technol 24(12):4697–4710
4. Kilper D et al (2011) Power Trends in communication networks. IEEE J Sel Top Quantum Electron 17(2):275–284
5. Kilper D, Guan K, Hinton K, Ayre R (2012) Energy challenges in current and future optical transmission networks. In: Proceedings of the IEEE, vol 100, No 5, pp 1168–1187
6. Zhuge Q et al (2013) Spectral efficiency-adaptive optical transmission using time domain hybrid QAM for agile optical networks. J Lightwave Technol 31(15):2621–2628
7. Ellis A, Suibhne NM, Saad D, Payne DN (2016) Communication networks beyond the capacity crunch. Philos Trans R Soc A 374:20150191
8. Bhopalwala M, Rastegarfar H, Kilper DC, Wang M, Bergman K (2016) Energy efficiency of optical grooming of QAM optical transmission channels. Opt Express 24(3):2749–2764. https://doi.org/10.1364/oe.24.002749
9. Udalcovs A, Schatz R, Wosinska L, Monti P (2017) Analysis of spectral and energy efficiency trade-off in sigle-line rate WDM links. J Lightwave Technol 35(10):1847–1857
10. Shieh A, Bao H, Tang Y (2008) Coherent optical OFDM: theory and design. Opt Express 16(2):841–859
11. Palkopoulu E et al (2013) Nyquist-WDM-based flexible optical networks: Exploring physical layer design parameters. J Lightwave Technol 31(14):2332–2339
12. Chandrasekhar S, Liu X (2012) "OFDM based superchannel transmission technology. J Lightwave Technol 30(24):3816–3823

13. Liu X et al (2014) Digital signal processing techniques enabling multi-Tb/s superchannel transmission. IEEE Signal Process Mag 31(2):16–24
14. Djordjevic IB (2018) Advanced optics and wireless communication systems. Springer, Berlin. ISBN 978-3-319-63151-6
15. Schmogrow R et al Real-time digital nyquist-WDM and OFDM signal generation: spectral efficiency versus DSP complexity. In: ECOC technical digest, Mo.2.A.4
16. Yu J, Zhang J (2016) Recent progress on high-speed optical transmission. Digital Commun. Netw. 2:65–76
17. Song M et al (2016) Flexible optical cross-connects for high bit rate elastic photonic transport networks. J Opt Commun Netw 8(7):Ai-26–AI-40
18. Pincemin E et al (2013) Multi-band OFDM transmission with sub-band optical switching. In: ECOC technical digest, Th.2.A.1
19. Sanjoh H et al Optical OFDM using frequency/time domain filtering for high spectral efficiency up to 1 bit/s/Hz. In: Proceedings of the optical society of America, ThD1
20. Winzer P (2014) An opto-electronic interferometer and its use in sub-carrier add/drop multiplexing. J Lightwave Technol 31(11):1775–2219
21. Hillerkus D et al (2010) Simple all-optical FFT scheme enabling Tbit/s real-time signal processing. Opt Express 18(9):9324–9340
22. Fabbri S et al 1st experimental demonstration of Tbit interferometric drop, add and extract multiplexer. In: ECOC technical digest, We.1.5.2
23. Fabbri S et al (2015) Experimental Implementation of an all-optical interferometric drop, add, and extract multiplexer for superchannels. J Lightwave Technol 33(7):1351–1357
24. Sygletos S et al All-optical add-drop multiplexer for OFDM signals. In: Proceedings of ICTON, We.A1.1
25. Wang Z et al (2011) Optical FFT/IFFT circuit realization using arrayed waveguide gratings and the applications in all-optical OFDM system. Opt Express 19(5):4501–4512
26. Ferreira, RJL, Dourado DM, Rodrigues MM, Rocha ML, Rossi SM, Pataca DM (2017) All-optical fast Fourier transform for processing an optical OFDM superchannel. In: SBMO/IEEE MTT-s IMOC 2017 technical digest
27. Jia W et al Methods for synchronization of superchannels in an optical node. In: ICTON technical digest, We.A1.6
28. Power MJ (2014) Clock recovery of phase modulated optical OFDM superchannel. In: OFC technical digest, W3F.1
29. Lee D et al (2008) All optical discrete Fourier transform processor for 100 Gbps OFDM transmission. Opt Express 16(6):4023–4028
30. Sygletos S et al (2014) A novel architecture for all-optical add-drop multiplexing of OFDM signals. In: ECOC technical digest, We.1.5.4
31. Reed GT et al (2010) Silicon optical modulators. Nat Photonics 4:518–526
32. Coldren LA (2010) High-performance photonic integrated circuits (PICs). In: OFC tutorial OWD1
33. Tait A et al (2013) The dream: an integrated electronic thresholder. J Lightwave Technol 31(8):1263–1272
34. Melloni A et al (2010) Tunable delay lines in silicon photonics: coupled resonators and photonic crystals, a comparison. IEEE Photonics J 2(2):181–194
35. Brian J et al (2009) Phase-controlled integrated photonic quantum circuits. Opt Express 17(16):13516–13525
36. Ellis A et al (2017) Performance limits in optical communications due to fiber nonlinearity. Adv Opt Photonics 9(3):429–503
37. Chang RW (1970) Orthogonal frequency multiplex data transmission system. US Patent 3488445 A (also published as DE1537555A1, DE1537555B2)
38. Weste N, Skellern DJ (1998) VLSI for OFDM. IEEE Commun Mag 36(10):127–131
39. Chang C-H, Wang CL, Chang YT (1999) A novel memory-based FFT processor for DMT/OFDM applications. In: 1999 IEEE international conference on acoustics, speech, and signal processing proceedings, vol 4, pp 1921–1924

40. Shieh W, Djordjevic I (2010) Orthogonal frequency division multiplexing for optical communications. Academic Press, Elsevier. ISBN 978-0-12-374879-9
41. Prasad R (2004) OFDM for wireless communication systems. Artech House, Boston. ISBN 1-58053-796-0
42. Ferreira RJL, Rocha ML, Ranzini SM (2013) System performance evaluation of an optical superchannel originated from different optical comb generation techniques. J Microw Optoelectron Electromagnet Appl 12(SI-2):66–78
43. Pataca DM, Simões FD, Rocha ML (2011) Optical frequency comb generator for coherent WDM system in Tb/s applications. In: IEEE/SBMO IMOC technical digest
44. Simões FD, Pataca DM, Rocha ML (2012) Design of a comb generator for high capacity coherent-WDM systems. IEEE Lat Am Trans 10(3):1690–1696
45. Pataca DM, Carvalho HH Adami CBF, Simões FD, Oliveira JCRF (2012) Transmissão de um supercanal OFDM de 1,12 Tb/s por 452 km com eficiência espectral de 4 b/s/HZ. In: SBrT technical digest
46. Yu J et al (2012) Generation of coherent and frequency-locked multi-carriers using cascaded phase modulators for 10 Tb/s optical transmission system. J Lightwave Technol 30(4):458–465
47. Maher R, Anandarajah PM, Ibrahim SK, Barry LP, Ellis AD, Perry P, Phelan R, Kelly B, O'Gorman J (2010). Low cost comb source in a coherent wavelength division multiplexed system. In: ECOC technical digest, P3.07, Torino, Italy
48. Kawanishi T et al (2004) Optical frequency comb generator using optical fiber loops with single-sideband modulation. IEICE Electron Express 1(8):217–221
49. Pataca DM et al (2011) Optical frequency comb generator for coherent WDM system in Tb/s applications. In: SBMO IEEE MTT-S IMOC technical digest
50. Pataca DM, Gunning P, Rocha ML, Lucek JK, Kashyap R, Smith K, Moodie DG, Davey RP, Souza RF, Siddiqui AS (1997–1998) Gain-switched DFB lasers. J Microw Optoelectron Electromagn Appl 1(1):44–63
51. Anandarajah PM et al (2011) Generation of coherent multicarrier signals by gain switching of discrete mode lasers. IEEE Photonics J 3(1):112–122
52. Browning C et al (2011) Performance of 10 Gb/s direct modulation OFDM by optical injection using monolithically integrated discrete mode lasers. Opt Express 19(26):B289–B294
53. Zhou R et al (2011) 40 nm wavelength tunable gain-switched optical comb source. Opt Express 19(26):B415–B420
54. Herbert C et al (2009) Discrete mode lasers for communication applications. IET Optoelectron 3(1):1–17
55. Cooley J, Tukey J (1965) An algorithm for the machine calculation of complex fourier series. Math Comput 19(90):297–301
56. Marhic ME (1987) Discrete Fourier transforms by single-mode star networks. Opt Lett 12(1):63–65
57. Siegman AE (2001) Fiber fourier optics. Opt Lett 26(16):1215–1216
58. Bouziane R et al (2011) Optimizing FFT precision in optical OFDM transceivers. IEEE Photonics Technol Lett 23(20):1550–1552
59. Gidddings RP et al (2009) First experimental demonstration of 6 Gb/s real-time optical OFDM transceivers incorporating channel estimation and variable power loading. Opt Express 17(22):19727–19738
60. Yang Q et al (2009) Real-time reception of multi-gigabit coherent optical OFDM sinals. Opt Express 17(10):7985–7992
61. Ma Y, Yang Q, Tang Y, Chen S, Shieh W (2009) 1-Tb/s per channel coherent optical OFDM transmission with subwavelength bandwidth access. In: OFC technical digest, PDPC1, pp 1–3
62. Palushani E et al (2014) All-optical OFDM demultiplexing by spectral magnification and band-pass filtering. Opt Express, 22(1):136–144. https://doi.org/10.1364/oe.22.000136
63. Puntsri K et al (2017) Experimental demonstration of 1024-IFFT FPGA implementation with 3.98 Gbps throughput for CO-OFDMA-PON transmitters. In: 5th international electrical engineering congress, Pattaya, Thailand, March 2017

64. Chandrasekhar S, Liu X (2009) Experimental investigation on the performance of closely spaced multi-carrier PDM-QPSK with digital coherent detection. Opt Express 17:21350–21361
65. Ellis AD, Gunning FCG (2005) Spectral density enhancement using coherent WDM. IEEE Photonics Technol Lett 17:504–506
66. Mueller K, Muller M (1976) Timing recovery in digital synchronous data receivers. IEEE Trans Commun 24(5):516–531
67. Yang B et al (2000) Timing recovery for OFDM transmission. IEEE J Sel Areas Commun 18(11):2278–2291
68. Gopal et al (2013) 40 Gbit/s all-optical signal regeneration with SOA in Mach-Zehnder configuration. IOSR J Electron Commun (IOSR-JECE) 6(2):33–35
69. Lowery AJ et al (2017) Photonic circuit topologies for optical OFDM and nyquist WDM. J Lightwave Technol 35(4):781–791
70. Deen MJ, Basu PK (2012) Silicon photonics: fundamentals and devices, 1st edn. Wiley, Chichester
71. Reed GT, Mashanovich G, Gardes FY, Thomson DJ (2010) Silicon optical modulators. Nat Photonics 4(8):518–526
72. Hartmann W et al (2015) 100 Gbit/s OOK using a silicon-organic hybrid (SOH) modulator. In: ECOC 2015 technical digest
73. Wolf S et al (2015) DAC-less amplifier-less generation and transmission of QAM signals using sub-volt silicon-organic hybrid modulators. J Lightwave Technol 33(7):1425–1432
74. Wolf S et al (2016) An energy-efficient 252 Gbit/s silicon-based IQ-modulator. In: OFC technical digest
75. Koos C et al (2016) Silicon-organic hybrid (SOH) and plasmonic-organic hybrid (POH) integration. J Lightwave Technol 34(2):256–268
76. Yu H, Hogchen Y, Chen H, Chen M, Yang S, Xie S (2016) All-optical OFDM demultiplexer based on an integrated Silicon-on-Insulator Technique. IEEE Photonics J 8(1)